EXPERIMENTAL INVESTIGATION OF A KW SCALE ABSORPTION POWER CYCLE WITH LIBR SOLUTION

Vaclav Novotny[1,2]*, Jan Spale[1,2], Jan Pavlicko[1,2], David J. Szucs[1], Michal Kolovratnik[2]

[1]Czech Technical University in Prague, University Centre for Energy Efficient Buildings,
Trinecka 1024, Bustehrad, 27343, Czech Republic

[2]Czech Technical University in Prague, Faculty of Mechanical Engineering, Technicka 4, Praha 6, 16607, Czech Republic

*Corresponding Author: vaclav.novotny@cvut.cz

ABSTRACT

Absorption cycles have been proposed not only for cooling but also for power generation. Most common is then Kalina cycle utilizing water-ammonia mixture working fluid. Other working fluids theoretically may provide thermodynamic benefits, have only rarely been examined experimentally. This work reports on, to the authors' knowledge, the world's first absorption power cycle using salt solution (here aqueous solution of LiBr), known so far only from absorption cooling. The system with a design power output of around 300 W features solutions such as a nylon 3D printed turbine or measurement of temperature glide during phase change in the heat exchangers.

This work is focused on an analysis of the experimental performance of the system. The measured turbine efficiency reached 25% with a potential for much higher values with better design. Over the range of explored conditions, if 65% expander performance was assumed, the maximal cycle efficiency could be around 4.5% and utilization efficiency 0.5%.

1   INTRODUCTION

Utilization of low temperature heat sources, especially of waste heat, efficiently has been a goal of many research activities. The traditional method widely considered and applied for higher temperatures, ORC, often doesn't reach at such low temperatures sufficient efficiency for commercial application. Moreover, the requirements for heat rejection rise significantly as the heat source temperature and efficiency decreases, and thus the relative amount of rejected heat against power output rises. The ideal cycle for utilization of low temperature is a trilateral cycle with a gradual increase of working fluid temperature along with the heat input, minimizing the irreversibilities. (DiPippo, 2012; An *et al.*, 2016; Novotny and Kolovratnik, 2017) Several methods to approach the trilateral cycles have been proposed, including the use of zeotropic working fluids with a temperature glide during phase change. Absorption power cycles are one of these systems, where many works in the past suggested the use of water-ammonia mixture and several plants were built (Kalina, 1985; Zhang, He and Zhang, 2012; Macwan, 2013).
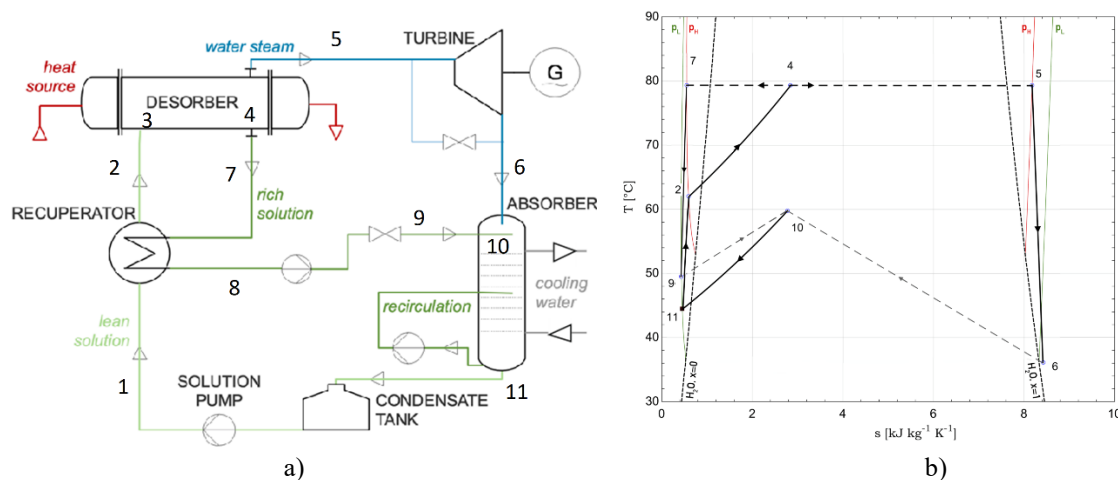
Another possible working fluid is a water-LiBr solution which was found to have theoretical advantages for very low temperatures and the prospect of the efficient unit for power outputs even down to kW scale as a result of low system pressures. (Novotny *et al.*, 2016; Novotny and Kolovratnik, 2017) The proposed working fluid is commonly applied in absorption chillers (Herold, Radermacher and Klein, 1996), but no previous experimental report of use as a power cycle has been found until now.

2   TEST RIG

In order to verify the real applicability of the proposed cycle with the LiBr solution, an experimental system has been proposed. First experimental considerations (Novotny *et al.*, 2017) and unsuccessful trials of low pressure flow boiling with pure water (Novotny, Suchna and Kolovratnik, 2018) led to the design of a proof of concept system of the cycle with a nominal power output in hundreds of watts. Its design was in detail introduced in (Novotný *et al.*, 2019). Here the design is briefly reviewed, followed by details on instrumentation and operation.

2.1   Design

The experimental proof-of-concept APC system is illustratively shown on a simplified diagram in Figure 1a and a *Ts* diagram for illustration of the processes is in Figure 1b. As it is suggested by the first figure, it utilizes a shell & tube desorber (i.e. steam generator) as well as a shell & tube falling film absorber (LiBr solution flown on the outer surface of helically wound tubes and steam is absorbed). The working fluid in the desorber (steam generator in cooling cycle terminology) undergoes a partial phase change, ideally with temperature glide for good temperature profile match with the heat source. The produced pure water steam is due to the boiling point elevation in a superheated state (when considered separately from the solution, with which it is at vapour liquid equilibrium) and is routed to the expander and subsequently absorber. The rich solution leaves absorber at the saturated state is routed to the absorber in a separate line via a recuperator. While concepts with counter-flow low volume heat exchangers (as plate type) assume a separator downstream, our design follows a large volume exchanger design which already serves as a separator, as found in common absorption chillers. Note an additional pump in the rich solution line to overcome potentially excessive pressure losses in the line and nozzles in the absorber. In the absorber, the steam is absorbed into a subcooled liquid solution film flowing on a heat transfer surface where heat is removed into cooling water. In case of an insufficient absorption rate additional solution, a recirculation circuit is considered here with the solution nozzles in the half of the absorber's height.

Figure 1: APC experimental rig, (a) schematic diagram, (b) *Ts* diagram of the designed cycle extended to saturation vapour and liquid lines of LiBr solution at high and low system pressure and of water

Major design parameters are summarized in Table 1 and in detail are described in (Novotný *et al.*, 2019). The overall configuration of the system is shown in Figure 2. Note especially the very low pressures of the turbine inlet and outlet. Also, as the device serves as the proof of concept, some components, especially the absorber, are oversized, and the device is built on two floors so that every part of the system is accessible for the commissioning.

The main phenomena to be verified by this system are at first of course for the overall operation, but also actual temperature profile in the heat exchangers with temperature glide (both desorber and

absorber have inserted multiple temperature probes along the flow direction) and last but not least feasibility of plastic 3D printed turboexpanders.
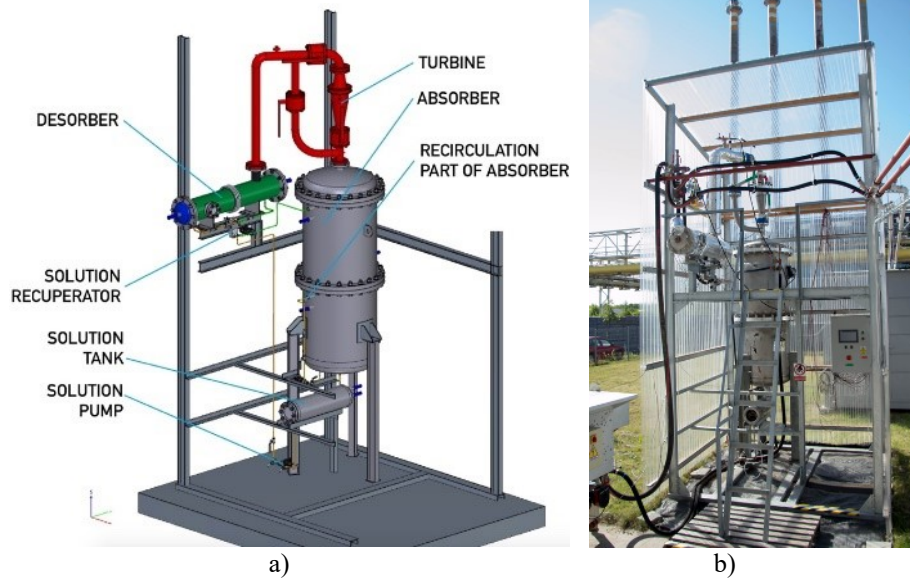

a)   b)

Figure 2: APC experimental rig, (a) 3D model of the system, (b) photograph of the system

TABLE 1. Main design parameters of the APC rig

Heat source & sink fluid	*water*		
Inlet temperature of the heat source	T_{hs}	90	*°C*
Heat input	Q_{in}	20	*kW*
Inlet temperature of the cooling water	T_{cw}	30	*°C*
Working fluid	*LiBr+H2O 35% (LiBr wt., lean) / 50% (rich)*		
Lean LiBr solution mass flow	$\dot{m}_{lean}$	0.026	*kg s⁻¹*
Vapour mass flow	$\dot{m}_{vap}$	0.008	*kg s⁻¹*
Turbine inlet pressure	P_{HP}	13.38	*kPa*
Turbine outlet pressure	p_{LP}	5.99	*kPa*
Turbine isentropic power output	W_{is}	840	*W*
Turbine design power output	W_{turb}	370	*W*
Design parasitic load (incl. cooling water pump and fan)	W_{paras}	116.2	*W*
Design cycle / system / utilization efficiency	$\eta_c/\eta_{syst}/\eta_u$	1.9 / 1.3 / 0.2	*%*

2.2 Instrumentation

In the APC rig, most of the measurements were taken and recorded via PLC system AS332T-A with measuring cards for RTD temperature sensors, voltage and current input. Additional temperature sensors for temperature glide were measured via Labview (cRio module). The turbine load was controlled via an in-house built DC load (output current was rectified first) system, which included a PID regulator to keep set rotational speed. This system also recorded the voltage and current along with rotational speed based on produced AC current frequency. Some details about this method can be found, for example, in (Spale *et al.*, 2021).

A simplified PFID showing the overall layout along with the position and types of measurements within the system is shown in Figure 3. It also shows design thermodynamic properties in respective streams. The details of the sensors for the measured variables are summarized in Table 2.
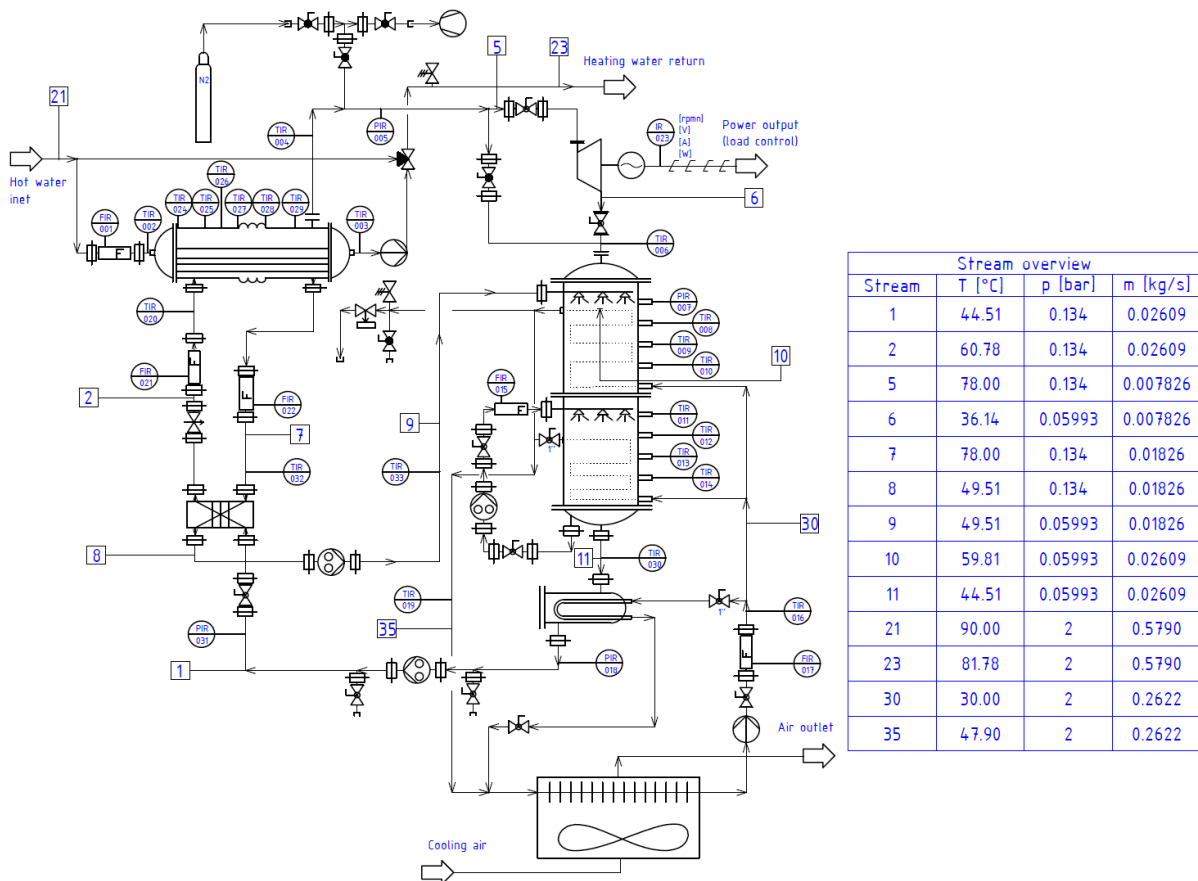
Figure 3: APC experimental rig simplified PFID

The stream overview table from the figure:

Stream	T [°C]	p [bar]	m [kg/s]
1	44.51	0.134	0.02609
2	60.78	0.134	0.02609
5	78.00	0.134	0.007826
6	36.14	0.05993	0.007826
7	78.00	0.134	0.01826
8	49.51	0.134	0.01826
9	49.51	0.05993	0.01826
10	59.81	0.05993	0.02609
11	44.51	0.05993	0.02609
21	90.00	2	0.5790
23	81.78	2	0.5790
30	30.00	2	0.2622
35	47.90	2	0.2622

Table 2: Test rig sensors and transducers

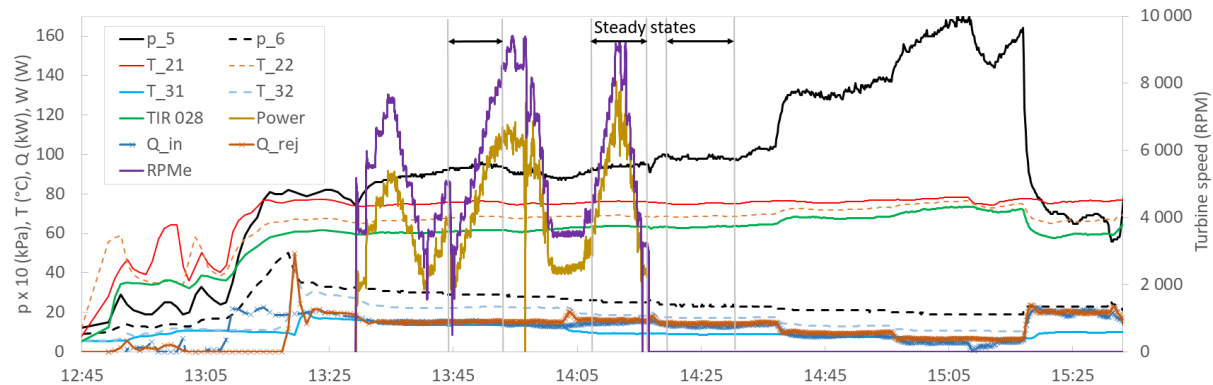| Parameter	Type	Range	Error
Pressure	Ceramic capacitive DMP331	0-400 kPa 0-200 kPa	0.35% FS, 0.10% FS
Temperature	Pt100 RTD (4 wire)	-50 - 200°C	0.5% + 0.3°C
Volumetric flowrate (LiBr solution)	Vortex LIQUI-VIEW Base LVB-06-A	0.5-10 l/min	<1% FS
Volumetric flowrate (hot/cold water)	Vortex LIQUI-VIEW Base LVB-20-A, LVB-15-A	5-85 l/min 3.5-50 l/min	<1% FS
Generated voltage	Voltage divider +Arduino A/D	0-60 V	2% + 0.03 V
Generated current	Arduino A/D via U drop (1 block)	0-30 A	2% + 0.02 A
Turbine rotation speed	Electrical frequency via Arduino A/D	2k-100k rpm	~20 rpm (@ 10k rpm)

2.3 Operation

Before each test, the system was evacuated, and after each test campaign, the rig was filled with nitrogen to slightly above ambient pressure to prevent oxygen intrusion and potential corrosion. The tests were performed for ranges of basic solution concentration of 54% (as purchased) and 50%, 45% and 40% and additionally during commissioning with pure distilled water. During the experimental tests, conditions of the cycle were set. The cycle operating with the turbine has two degrees of freedom, speed of the main pump and of the rich solution pump. When the bypass valve was used instead of the turbine, its opening simulated the turbine's swallowing capacity and thus provided one another degree of freedom.

The pumps were operated in a way that the recirculation pump was set to run at a certain constant speed, while the lean solution pump was (manually) controlled to provide a constant liquid level in the desorber. The opposite way of control has proven to be unreliable as at certain states; the liquid solution stopped returning to the storage tank (suspected crystallization issues though there should have been a

margin from the crystallization concentration. This phenomenon might deserve deeper focus in the future. The control of the pump, together with the high time constant of the system, sometimes caused large departures from steady-state liquid flows. At least partial correction for these discrepancies is provided in the next chapter.

The heat source was heating water taken as part of the output of biomass-fired ORC units, either a 50 kW$_{th}$ version as described in (Mascuch *et al.*, 2018) or its scaled up 120 kW$_{th}$ version. Due to the unit's settings and partly heat losses in the heat input pipes, the heat source temperature was most of the time between 75 and 85°C, while it could be further decreased by a three-way valve mixing in the return water. The spread of explored heat source temperature was 67-88°C. The heat sink was given by cooling water which rejected the heat into the air in an air cooler, and temperature depends on ambient conditions. The range of the explored cooling water temperatures was 11-46°C. The range of temperature difference between heat source inlet and cooling water inlet was 38-71K, but bear in mind that the mass flow rates differed as well, between 0.15-0.87 kg/s at the heat source side and 0.27-0.47 kg/s at the cooling water. The experimental campaigns with LiBr solution were performed in total in 9 days between June and November 2020. A sample of recording of the selected data from the operation is in Figure 4, with a distinct period of turbine operation, while the bypass was operated at the rest of the time. The selected operation data of the steady state periods are summing up for about 20 hours out of which the turbine was in operation for more than 6 hours.

Figure 4: Example of the record of selected parameters from the APC operation with an indication of the selected steady-state periods with and without turbine operation (numbers correspond to the PFID)
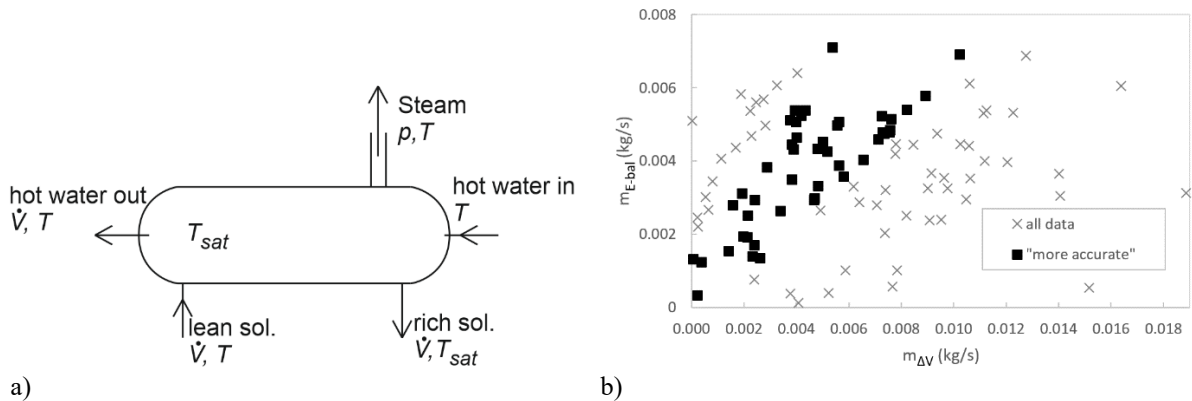
3 DATA EVALUATION

From the recorded data are selected time periods or rather a constant operation, evaluated primarily by the steadiness of the pressure levels. For further evaluation, the average values from these selected time periods were obtained, and each value was treated as an operational state.

The mass flow rate cannot be directly evaluated from the volumetric flow rate of the liquid streams. The reason is that the density is a function of LiBr concentration, which is not directly measured. Therefore mass and energy balance equation of the desorber is used with the inputs, outputs and measuring point according to Figure 5a. The assumption taken is that the rich solution leaving the absorber is at the saturated rich solution temperature, thus its concentration is given. As the solution is boiling within the desorber, this assumption should be accurate. A slight difference in results is obtained if mass balance is applied to both solution and each component or, e.g. energy balance of separation (from calculated 2 phase fluid quality). Using the energy balance also helps to smoothen and to lower the impact of transient effects affecting the flowrate during cycle control (rising or falling of desorber liquid level) and from volumetric flowrate measurement inaccuracies.

The resulting graph in Figure 5b shows the discrepancy between the values obtained from energy balance and the difference from the two measured volumetric flow rates. In order to select data with higher quality, values with relative difference smaller than 40% or absolute difference smaller than

0.015 kg/s were selected. Fluid properties are evaluated using the REFPROP database for water and using formulation (Kim and Ferreira, 2004) for the LiBr solution.

Figure 5: Schematic diagram of desorber parameters used in the evaluation of steam mass flow rate (a) and graph of steam mass flow rate obtained by the difference in measured volumetric flow and from the energy balance (b)

The turbine efficiency is evaluated with respect to the isentropic power. The efficiency is evaluated both for the produced electrical power output (electrical efficiency), but isentropic efficiency is from the power output evaluated as well. As the measured power is in the form of electricity, obtaining mechanical power output has been done by using generator efficiency evaluated for each operation state. The generator efficiency is obtained from characteristics provided by an eCalc[1] tool, which includes performance parameters of a wide range of aeromodelling BLDC motors. This tool was used to obtain torque–rotational speed–efficiency dependencies, which were then applied. Additionally, a nearly constant voltage drop on the rectifier was taken into account.

For the system itself, the important parameter is not just cycle efficiency (specified in Equation (1)), but also a utilization efficiency (with respect to heat source heat content). Reference for the utilization efficiency was taken as cooling water inlet temperature $T_{cw,in}$ as shown in Equation (2). Only the gross efficiency (excluding all parasitic load) was evaluated at this point. The unit was in most of the time, operated with the bypass valve, only simulating the turbine. In order to assess the potential of the cycle in general, a hypothetically achievable expander efficiency η_{turb} of 65% has been assumed as safely realistic for such small systems based on (Weiss *et al.*, 2017; Weiß *et al.*, 2019). The cycle parameters are then calculated with this expander efficiency value.

When the turbine was in operation the system produced an actual power output. This DC (after rectification) power output, i.e. including turbine isentropic efficiency, generator efficiency and rectifier diode efficiency (voltage drop), is then used to evaluate actual system efficiency as shown in second expressions in Equations (1) and (2). The number of operating points with turbine is lower with one reason being the given turbine's swallowing capacity.

$$\eta_c = \frac{\dot{W}_{turb}}{\dot{Q}_{in}} = \frac{\dot{m}_{steam} \cdot (h_{turb,in} - h_{turb,out,is}) \cdot \eta_{turb}}{\dot{m}_{source} \cdot (h_{source,in} - h_{source,out})} \bigg|_{\eta_{turb}=65\%} \quad OR \quad \eta_c = \frac{\dot{W}_{turb,el,measured}}{\dot{Q}_{in}} \tag{1}$$

$$\eta_u = \frac{\dot{W}_{turb}}{\dot{Q}_{source}} = \frac{\dot{m}_{steam} \cdot (h_{turb,in} - h_{turb,out,is}) \cdot \eta_{turb}}{\dot{m}_{source} \cdot (h_{source,in} - h_{source}(T=T_{cw,in}))} \bigg|_{\eta_{turb}=65\%} \quad OR \quad \eta_c = \frac{\dot{W}_{turb,el,measured}}{\dot{Q}_{source}} \tag{2}$$

Uncertainty analysis of the systematic error was performed for the cycle parameters as well. Partial derivatives of the resulting parameters were substituted by differences with a specified step from the measured value. Since the measured temperature and pressure differences are rather small and the method of obtaining turbine mass flow rate and solution concentration are not straight forward,

---

[1] https://www.ecalc.ch/torquecalc.php

evaluated uncertainties are in the order of often dozens percent of the reported value, with the median of the uncertainty of the main parameters reported in Table 3 (including possible outliers). This highlights the fact that the results need to be taken as the report of the first proof of concept operation and for higher accuracy a different approach to the instrumentation can be taken in the future. Note the specifically low value for rich solution concentration as the solution at the desorber outlet is saturated and only one pressure and temperature affects the resulting value. Similarly the measured utilization efficiency is calculated from higher temperature difference and from directly measured power output, even though the overall values are low.

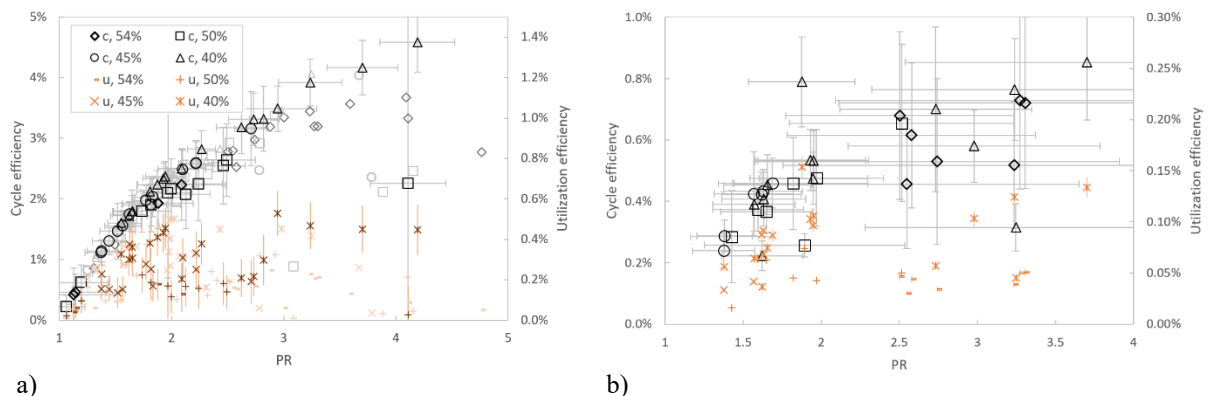**Table 3:** Median uncertainties of major cycle parameters

Parameter	Uncertainty (%)	Parameter	Uncertainty (%)
Cycle efficiency (η_{turb}=65%)	17.8	Steam mass flow rate	35.9
Utilization efficiency (η_{turb}=65%)	39.9	Solution flowrate	25.9
Cycle efficiency (measured $\dot{W}_{turb,el}$)	22.0	Rich solution concentration	1.3
Utilization efficiency (m. $\dot{W}_{turb,el}$)	7.2	Lean solution concentration	6.3
Pressure ratio	20.4	Concentration change	34.6

4 EXPERIMENTAL RESULTS

The experimental performance has been explored mainly from three points of view, regarding parameters of the cycle, the performance of the plastic 3D printed turboexpander and obtained actual temperature profiles during the phase change with the temperature glide.
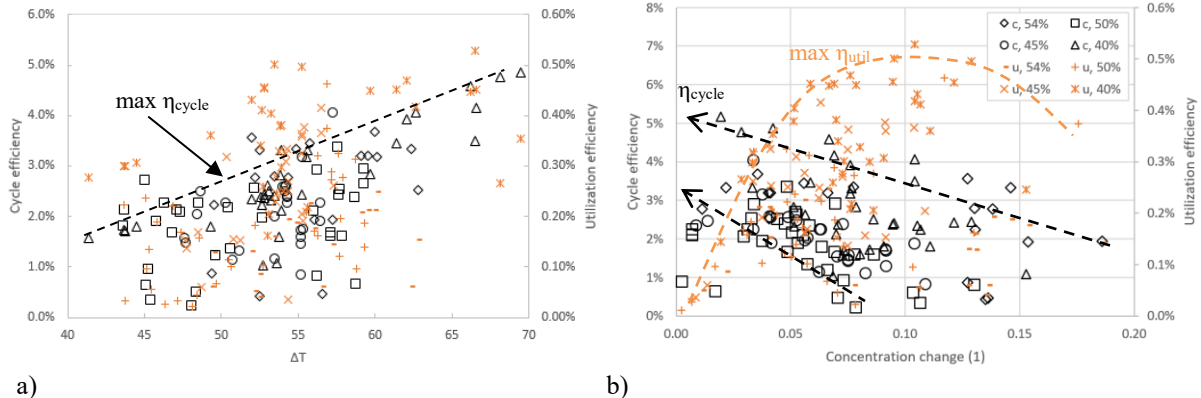
4.1 Cycle parameters

The cycle and utilization efficiency for assumed expander efficiency of 65% (or rather efficiency potential) is plotted for these states in Figure 6 as a function of cycle pressure ratio and distributed according to the calculated concentration difference. The operation states recorded as more accurate are highlighted with rich colour. The second graph shows the same parameters but for actual expander electrical output. In these graphs are shown the uncertainties values (in Figure 6a only for the more accurate states) for illustration that the results are mostly illustrational rather than highly precise.

a)   b)

Figure 6: Cycle and utilization efficiencies (*c* and *u*) as a function of charged LiBr concentration (40-54%) and cycle pressure ratio (*PR*). Values for hypothetical 65% expander efficiency with "more accurate" states in bold (a) and actually measured parameters with a current plastic turbine (b)

Note that the operation points are, however, recorded over a range of heat source and heat sink temperatures and mass flow rates. In order to generalize the data with respect to the temperature potential, Figure 7a shows the same data points as a function of the temperature difference between the heat source and heat sink inlets. It is not an exhaustive range of possible operation states, but the general trend is seen that the maximum cycle efficiency is independent of the fluid charge concentration. The highest utilization efficiency is a domain of the lowest explored concentration, where is the highest potential for concentration change from lean to rich solution.

Multiple values for the same temperature difference (e.g. around 67°C, c,40%) are partly caused by the high uncertainty, partly the temperatures of heat source and sink can differ. Another cause is in different ratio between the lean and rich solution flowrate (another degree of freedom for the APC control). This fact suggests that the optimal control strategy is also not as straight forward as for simple cycles such as ORC.
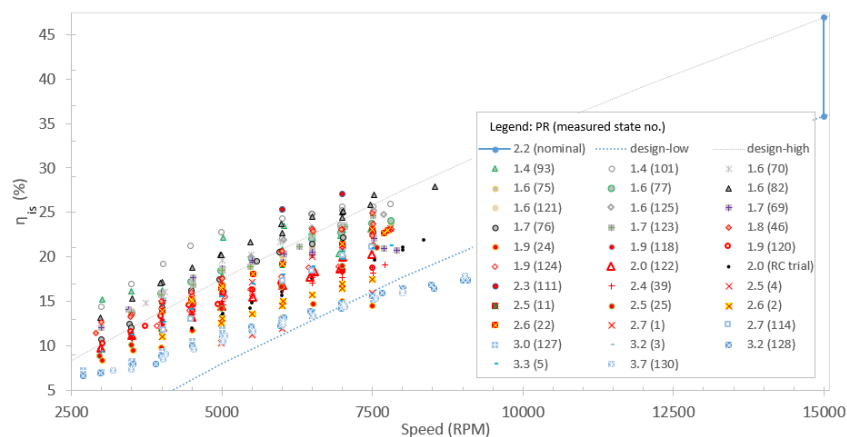

a)   b)

Figure 7: Cycle and utilization efficiencies (*c* and *u*) as a function of charged LiBr concentration (40-54%) and of the temperature difference *ΔT* between the heat source and heat sink (a) and of a concentration change in the cycle (b), all for hypothetical 65% expander efficiency

The concentration change is furthermore used for plotting the data Figure 7b. Here we can see a confirmation of the thermodynamic models that the highest cycle efficiency is associated with lower values of concentration change (but not the very lowest, particular optimum exists). On the other hand, the utilisation efficiency increases with the concentration change with a possible optimum at somewhat higher values. Thus, a drop in utilisation efficiency might come with a further increase in the concentration difference (if the operating conditions allow such a state).

4.2   Turboexpander performance

During the operation of the experiment, the expander was in operation between various pressure levels with the summary of all experimental characteristics in Figure 8. During the operation, a resonance frequency and related vibrations caused that the maximal turbine speed was around 8000-9000 rpm. The results confirm that the generally expected trend of decreasing efficiency with increasing the pressure ratio is valid. Even with the poor surface quality, the efficiency is mostly within boundaries provided by different loss models. This shows a high prospect of the plastic 3D printed concept with better engineering than was adopted for this proof of concept. Furthermore inspection after about a year in the environment with LiBr and more than 6 hours of operation, nor the turbine, nor the generator showed any signs of damage or corrosion.
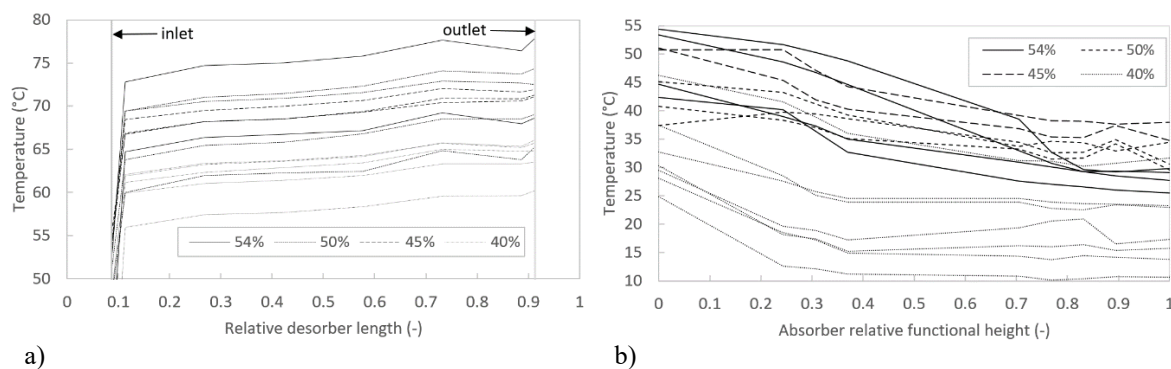

Figure 8: Measured turbine characteristics from APC operation and comparison with design

There are several reasons behind the very low efficiency of the tested turbine. One is surely the poor surface quality of the flow sections as for these first trials, no post-processing was applied and the surface is in the as-printed state. Second reason is the low velocity ratio, as it can be seen already from the design point at unreached 15 000 rpm and the theoretical optimum is around 30 000 rpm. Lastly, design was performed with loss models adopted from large steam turbines and no CFD optimization of the geometry has been performed. Altogether, there is clearly a potential for major improvement with more advanced design engineering than was adopted for this first proof of concept.

4.3   Temperature glide measurements

One of the objectives of the rig was to evaluate the temperature glide across the non-isothermal phase change during desorption and absorption, as high temperature change was suggested in the past for waste heat recovery. This glide for several selected operation cases is shown for both desorber and absorber in Figure 9. For the desorber, there is a measured temperature of the boiling solution as the temperature probes are placed under the liquid level. The recorded glide is significantly lower than theoretical yet still well measurable. A certain decrease of the glide was expected due to the large volume shell & tube exchanger with a nearly quiescent pool of the boiling solution. Interestingly, the glide doesn't much differ between the operation states with various solution charge LiBr concentration. Such a result is, however, in accord with results in Figure 7b, where no clear relation between concentration difference and charge solution concentration has been found. The lowest absolute absorber temperature values for some of the 40% concentration are caused only by the fact that ambient conditions allowed to achieve lower temperatures at these tests.

Figure 9: Measured temperature glide profiles in desorber (a) and absorber (both sections) (b)

In the case of the absorber, in most of the cases was operational only the upper half as the lower half designed as a backup if the absorption rate is insufficient. The measured temperature corresponds sometimes to the low pressure water vapour than to the liquid LiBr solution as the probes wetting by the solution cannot be fully assured due to the nature of the process. The inlet temperature shown is the turbine outlet vapour, while the first point of measurement is after a packing (for adiabatic absorption) and a small portion of cooling coils. Heat released during the adiabatic absorption may explain the temperature increase in some cases between the inlet and the first measurement. An increase in temperature in the bottom part may be associated with lower wetting of a specific probe by the solution when the steam has the higher temperature.

5   CONCLUSIONS

A proof of concept absorption power cycle unit with LiBr solution working fluid has been built and operated. To the authors' knowledge, the unit is a first power cycle with a salt solution experimentally operated. With the heat source temperature below 90°C, the maximum gross electrical cycle efficiency reached 0.8% and about 150 W. However, with a state of the art turboexpander, there is potential for maximal cycle efficiencies of almost 5% and heat source utilization efficiencies around 0.5%. A plastic 3D printed turboexpander has successfully applied. Current turbine efficiency limits of around 25% can be easily improved with a mechanical design allowing higher rotational speed and with surface polishing (the as-printed state was used for first tests). The temperature glide has been measured, even

though lower than theoretical, which was partly expected with the chosen desorber design. Overall, the experimental performance and results show the general feasibility of the concept.

REFERENCES

An, Q. *et al.* (2016) 'Categorization and analysis of heat sources for organic Rankine cycle systems', *Renewable and Sustainable Energy Reviews*. Elsevier, 64(October), pp. 790–805.

DiPippo, R. (2012) *Geothermal power plants : principles, applications, case studies, and environmental impact*. Oxford, UK: Butterworth-Heinemann.

Herold, K. E., Radermacher, R. and Klein, S. A. (1996) *Absorption chillers and heat pumps*. CRC press.

Kalina, A. I. (1985) 'Method of generating energy'. Google Patents.

Kim, D. S. and Ferreira, C. A. I. (2004) 'A Gibbs Energy Equation for LiBr/H2O Solutions', in *Proceedings of the 6th IIR Gustav Lorentzen Conference on Natural Working Fluids, Glasgow (UK)*.

Macwan, S. (2013) 'THE KALINA CYCLE- A Major Breakthrough in Efficient Heat to Power Generation', in *CHP2013 & WHP2013 Conference and Trade Show*.

Mascuch, J. *et al.* (2018) 'Experimental development of a kilowatt-scale biomass fired micro – CHP unit based on ORC with rotary vane expander', *Renewable Energy*.

Novotny, V. *et al.* (2016) 'Analysis and design of novel Absorption Power Cycle plants', in *ASME 2016 10th International Conference on Energy Sustainability, ES 2016, collocated with the ASME 2016 Power Conference and the ASME 2016 14th International Conference on Fuel Cell Science, Engineering and Technology*.

Novotny, V. *et al.* (2017) 'Design of Experimental Rig for Validation of Absorption Power Cycle Concept', *Energy Procedia*. Elsevier B.V., 105, pp. 4990–4996.

Novotný, V. *et al.* (2019) 'ABSORPTION POWER CYCLE WITH LIBR SOLUTION WORKING FLUID-DESIGN OF THE PROOF-OF-CONCEPT UNIT', in *5 th International Seminar on ORC Power Systems*. Athens.

Novotny, V. and Kolovratnik, M. (2017) 'Absorption power cycles for low-temperature heat sources using aqueous salt solutions as working fluids', *International Journal of Energy Research*, 41(7), pp. 952–975.

Novotny, V., Suchna, D. and Kolovratnik, M. (2018) 'Experimental rig for LiBr-water absorption power cycle - Design and first experimental results', in *AIP Conference Proceedings*.

Spale, J. *et al.* (2021) '3D printed radial impulse cantilever micro-turboexpander for preliminary air testing', in *AIP Conference Proceedings*. AIP Publishing LLC AIP Publishing , p. 070002.

Weiss, A. P. *et al.* (2017) 'EXPERIMENTAL INVESTIGATION OF A SUPERSONIC MICRO TURBINE RUNNING WITH HEXAMETHYLDISILOXANE', in *36th Meeting of Departments of Fluid Mechanics and Thermodynamics, 16th conference on Power System Engineering, Thermodynamics & Fluid Flow - PSE 2017*.

Weiß, A. P. *et al.* (2019) 'A micro-turbine-generator-construction-kit (MTG-c-kit) for small-scale waste heat recovery ORC-Plants', *Energy*. Elsevier Ltd, 181, pp. 51–55.

Zhang, X., He, M. and Zhang, Y. (2012) 'A review of research on the Kalina cycle', *Renewable and Sustainable Energy Reviews*. Elsevier, 16(7), pp. 5309–5318.

ACKNOWLEDGEMENT